



LAWRENCE
LIVERMORE
NATIONAL
LABORATORY

UEDGE Simulation of DIII-D Shot 141628 at 2490 msec

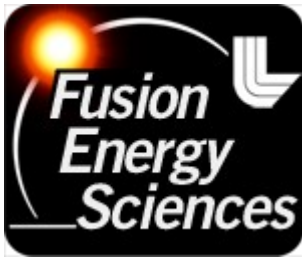
M. E. Rensink

September 21, 2010

Disclaimer

This document was prepared as an account of work sponsored by an agency of the United States government. Neither the United States government nor Lawrence Livermore National Security, LLC, nor any of their employees makes any warranty, expressed or implied, or assumes any legal liability or responsibility for the accuracy, completeness, or usefulness of any information, apparatus, product, or process disclosed, or represents that its use would not infringe privately owned rights. Reference herein to any specific commercial product, process, or service by trade name, trademark, manufacturer, or otherwise does not necessarily constitute or imply its endorsement, recommendation, or favoring by the United States government or Lawrence Livermore National Security, LLC. The views and opinions of authors expressed herein do not necessarily state or reflect those of the United States government or Lawrence Livermore National Security, LLC, and shall not be used for advertising or product endorsement purposes.

This work performed under the auspices of the U.S. Department of Energy by Lawrence Livermore National Laboratory under Contract DE-AC52-07NA27344.



MEMORANDUM

To: DIII-D 2010 Joint Research Task Team
From: M E Rensink
Date: 16 September 2010
Subject: UEDGE simulation of DIII-D shot 141628 at 2490 msec

1 Introduction

Experiments on CMOD and DIII-D have been run for similar plasma shapes to facilitate comparison of divertor heat loads. We have also run UEDGE simulations of the edge plasmas for these similarity shots. As previously identified, the relevant time slices are CMOD shot number 1100212024 at 1360 msec and DIII-D shot number 141628 at 2490 msec. The corresponding plasma shapes are shown in Figure 1 together with the divertor target surfaces. The principal qualitative difference is in the outer target configuration which is "open" for DIII-D and "closed" for CMOD.

2 Discharge Description

DIII-D discharge 141628 is part of a series of shots for inter-machine comparisons for heat flux scaling. It has a shape that CMOD and NSTX can run. It was run with 3 + 4 gyrotron-equivalent beams running at 43 kV accelerating voltage, and no gyrotrons. Total power input was about 2.0 MW with 1.6 MW from beams and 0.4 MW ohmic heating. $B_t = 1.7$ T, $I_p = 0.76$ MA. The timeslice 2500 msec was selected for simulation because the plasma configuration was not "breathing" so TS data could be averaged over a longer time. This time slice is in the middle of an X-point sweep. Several diagnostics on the experiment can be used to benchmark the UEDGE simulations: Thomson Scattering (TS), reflectometer and

Charge-Exchange Recombination (CER) profiles near the outer midplane, Infra-Red TV (IRTV) heat flux profiles on the divertor plates and visible TV images of D α and CIII radiation in the divertor region.

3 UEDGE Inputs

The UEDGE mesh is generated using data from the EFIT reconstruction for shot 141628 at 2490 msec. The scatter in the TS data did not justify re-locating the separatrix for this reconstruction. The mesh shown in Figure 2 was used for all UEDGE simulations in this report. The mesh contains 61 cells in the poloidal direction and 23 cells in the radial direction. The divertor target surfaces are quite simple in this configuration, so mesh resolution should not be an issue.

The UEDGE simulations solve time-dependent fluid equations for the plasma and neutral species. Several model options are available. For DIII-D we include carbon impurities due to both physical and chemical sputtering in the divertor. Cross-field drifts are included, but for these simulations at an artificially reduced level of 10%. This allows the runs to converge more robustly during parameter variations. Later we will increase the drifts to full strength. Most of the simulations used spatially uniform anomalous radial transport coefficients with particle diffusivity $0.10 \text{ m}^2/\text{sec}$ and thermal diffusivities $0.25 \text{ m}^2/\text{sec}$ for electrons and ions. Radially varying particle diffusivity can be used to introduce a transport barrier near the separatrix and control the upstream density profile. This was briefly explored. Core plasma boundary conditions are set to be consistent with experimental data: for most of these simulations the plasma density is $6e19 /\text{m}^3$ and total input power is 1.6 MW.

4 UEDGE Base Case Results

We have a base case simulation, JRT25a, with input parameters described in the previous section. Here we compare simulation results from this case with the available experimental data. In the simulation we observe that the plasma is detached from the inner target with temperatures less than 1 eV at the plate; the power flow to the outer target is sheath-limited with high temperature (48 eV) at the outer strike point. Due to the "open" divertor configuration, recycling neutrals produced by SOL ions striking the outer divertor plate are directed away from the separatrix. This reduces the recycling near the strike point and leads

to higher electron temperature. Impurities radiate about 0.7 MW of the total 1.6 MW input power. For this simulation there is a large ion current (700 Amps) from the core plasma which ultimately gets pumped at the vessel wall, mainly in the divertor region. This large particle throughput in steady state should be consistent with beam fueling of the core plasma. We have not yet made this assessment for the gyrotron-equivalent beams used in this discharge.

The simulated midplane electron density profile (in units of $10^{20} /\text{m}^3$) is compared with TS data and reflectometer data in Figure 3. The horizontal axis is the normalized magnetic flux. The "x" are TS data points and "o" are reflectometer data points; these do not seem to correlate very well. The simulated profile does not exhibit the pedestal characteristic of H-mode plasmas. One possible remedy is to use radially varying particle diffusivity, essentially introducing a particle transport barrier at the separatrix. This variation is discussed later in this report. Another remedy is to reduce the particle throughput for this simulation by reducing the wall pumping, but a change in the wall albedo (discussed later) did not have the desired effect.

The simulated midplane electron temperature is compared with TS data in Figure 4. The core boundary temperature in the simulation could be reduced by increasing the electron thermal diffusivity. The high degree of scatter in the TS data does not provide much of a constraint on the shape of the electron temperature profile in UEDGE simulation. The midplane ion temperature is even less constrained by the CER data in Figure 5. No attempt was made to extract more meaningful data from the automated CER data that was collected.

The simulated divertor heat flux is compared with IRTV data in Figure 6. The horizontal axis is normalized magnetic flux, ψ_{sin} , with $\psi_{\text{sin}} < 1$ in the private flux region and $\psi_{\text{sin}} > 1$ in the SOL region. The heat flux near the inner strike point is in "blue" and the heat flux near the outer strikepoint is in "red". The solid lines are the UEDGE simulations and the circles are the IRTV data points. The IRTV data shows a very weak peak on the outer target whereas the simulation has a strong peak of about $4 \text{ MW}/\text{m}^2$. In the simulation, global power balance shows 0.9 MW radiated by impurities, 0.2 MW radiated by hydrogenic species and 0.7 MW incident on the outer divertor plate.

The visible TV images of Dalpha radiation at 6356A and CIII radiation at 4650A provide clues as to the temperatures in the divertor region. The simulated Dalpha emissivity is compared with the emissivity deduced from camera image data in Figure 7. The simulated CIII emissivity is compared with that from camera data in Figure 8. Absolute intensities are not available from the camera images. The strong Dalpha emissivity (due to recombination?) on the inner divertor leg is indicative of a detached plasma in both the simulation and the camera data. The absence of a strong CIII emission at the inner target also indicates a low electron temperature in this region.

5 Parameter Variations

The base case described above could be made more realistic by adjusting some input parameters in the model, such as anomalous radial diffusivities, input power and drift strength. Some of these changes make it very difficult to advance the time-dependent fluid equations to a steady state solution. We have a few simulations that exhibit the effects of varying a single input parameter. These may be useful in guiding future modelling efforts.

5.1 input power

Simulation JRT25b had the input power increased from 1.6 MW to 2.0 MW relative to our base case, JRT25a. The peak electron temperature at the outer strike point increased from 48 eV to 82 eV, but no other significant changes were noted.

5.2 wall pumping

Simulation JRT26 had the outer wall albedo reduced from 0.98 in our base case to 0.95. This change did not affect the particle throughput because the neutral hydrogen density near the wall decreased and the net pumping by the wall was essentially unchanged. This did have the unexpected effect of reducing the level of carbon impurities because of reduced chemical sputtering by neutral hydrogen. The associated reduction in carbon radiation caused the inner leg of the divertor to re-attach.

5.3 drift strength

Simulation JRT15a had the drifts turned on relative to simulation JRT15. These runs did not include impurities. The drifts are artificially reduced to 10% of their classical value to allow easy convergence to steady state. At this level, the drifts do not significantly change the simulation. Further increases in drift strength will be necessary to assess the issue.

5.4 impurities

Simulation JRT15f included carbon impurities, whereas simulation JRT15a did not. The carbon is due to physical and chemical sputtering in the divertor region (target plates and private flux wall). The sputtering rates are those given by Haasz, et al. The impurities radiate about 0.7 MW of the total 1.6 MW input power. This has the effect of detaching the plasma from the inboard target where most of the power is radiated.

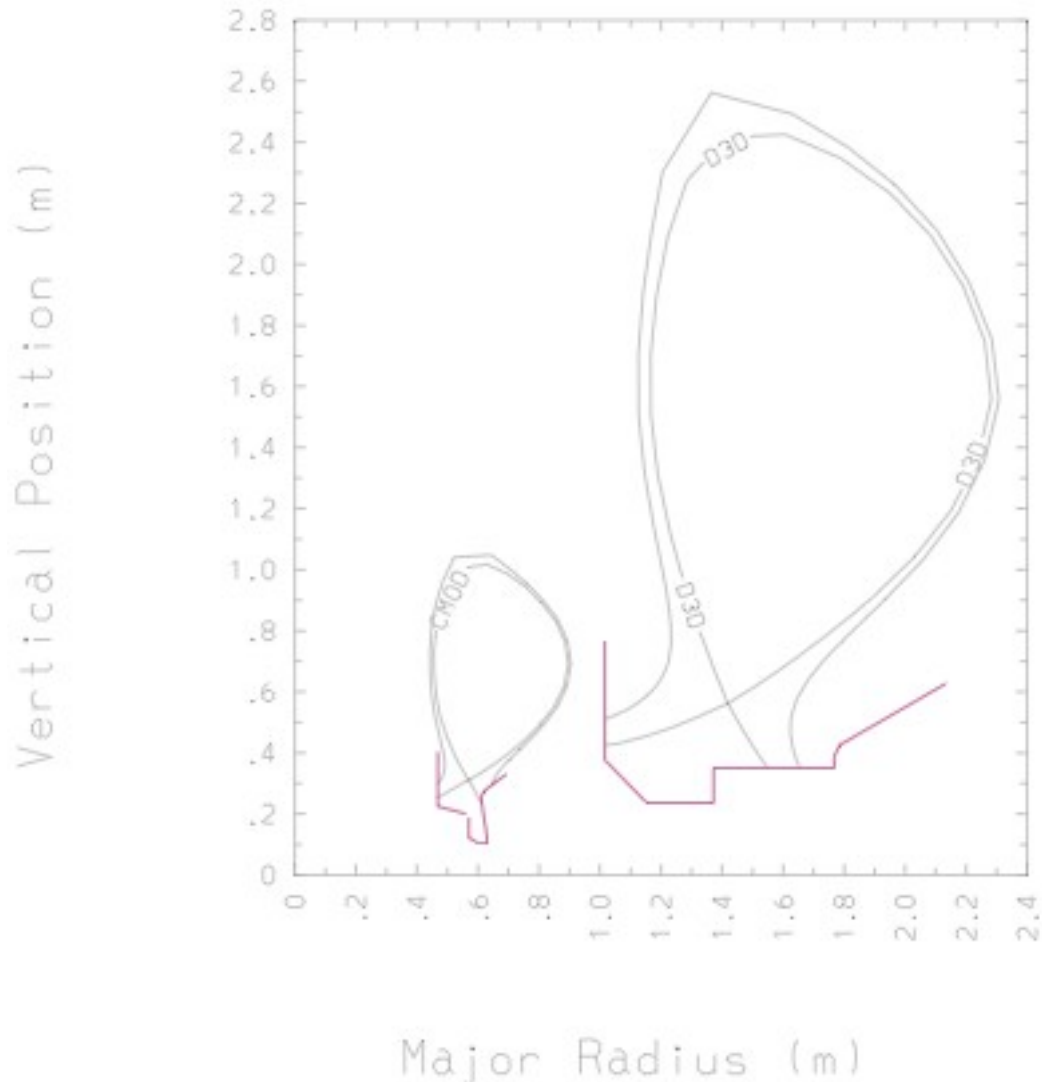
5.5 radially varying particle diffusivity

Most of the simulations use a spatially uniform particle diffusivity, $difniv=0.1 \text{ m}^2/\text{sec}$. An example is simulation JRT15 which had no drifts and no impurities. This simulation was re-run as JRT16 with a spatially varying particle diffusivity similar to that used by Porter in the CMOD simulations, i.e., the particle diffusivity was reduced to $0.015 \text{ m}^2/\text{sec}$ on flux surfaces within about 1 cm of the separatrix at the outboard midplane. The uniform diffusivity produces an upstream electron density which decreases linearly with radial position from the core boundary to the outer wall. In contrast, the varying diffusivity yields a flattened density profile in the core plasma and a rapid drop at the separatrix near the transport barrier. The reduced transport across the separatrix leads to reduced density and increased temperatures at the divertor plates.

6 Acknowledgement

This work performed under the auspices of the U.S. Department of Energy by Lawrence Livermore National Laboratory under Contract DE-AC52-07NA27344.

plasma shapes for CMOD and DIII-D



```

CMOD: plot zml.tyaptr,3) rml.tyaptr,3) scale=equal labels="CMOD"
plot zml.ny,3) rml.ny,3) scale=equal labels=blank
plot zplate1 rplate1 color=magenta thick=3 labels=blank
plot zplate2 rplate2 color=magenta thick=3 labels=blank
D30: plot zml.tusstr,3) rml.tusstr,3) scale=equal labels="D30"

```

Fig. 1: Comparison of CMOD and DIII-D plasma size and shape

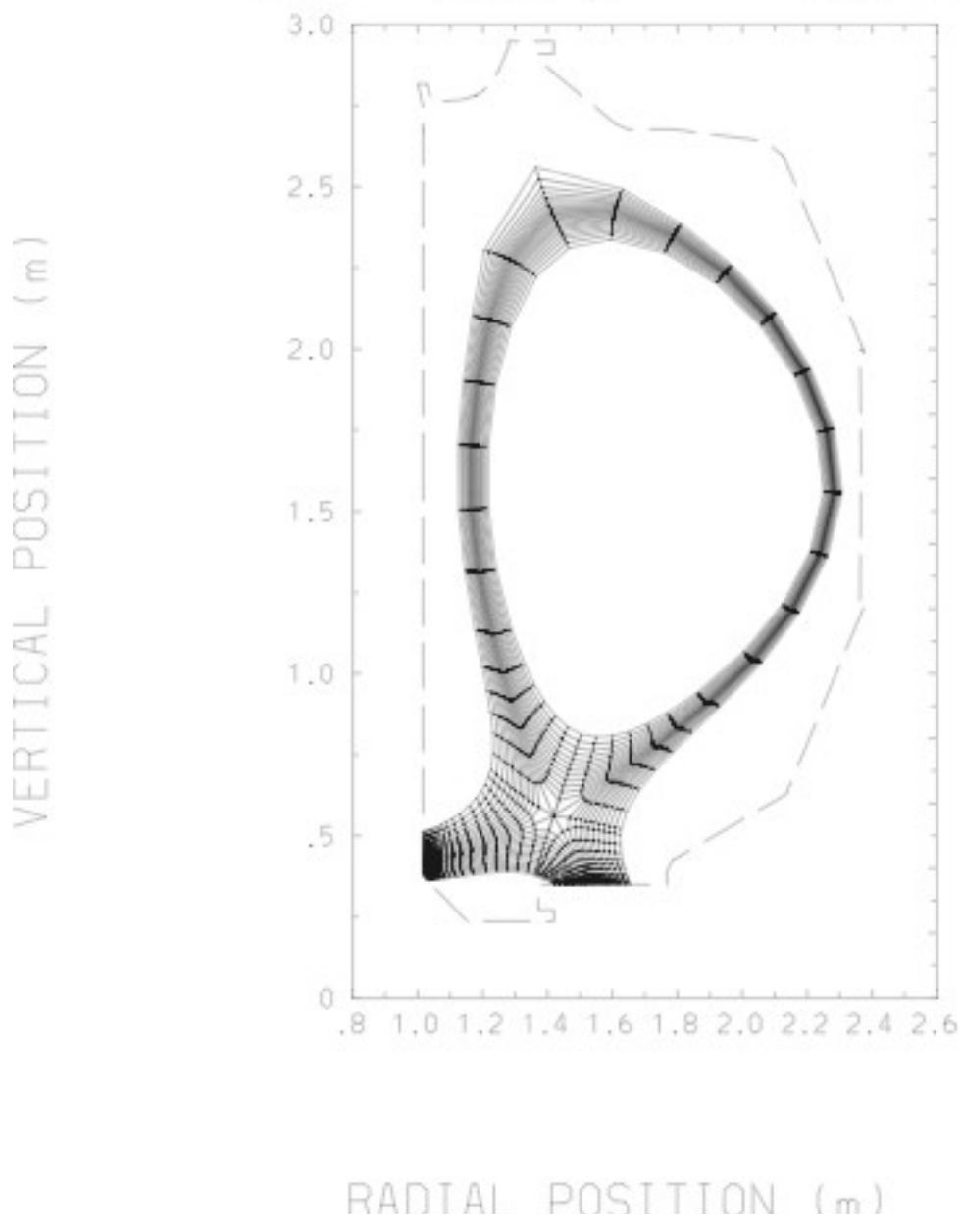
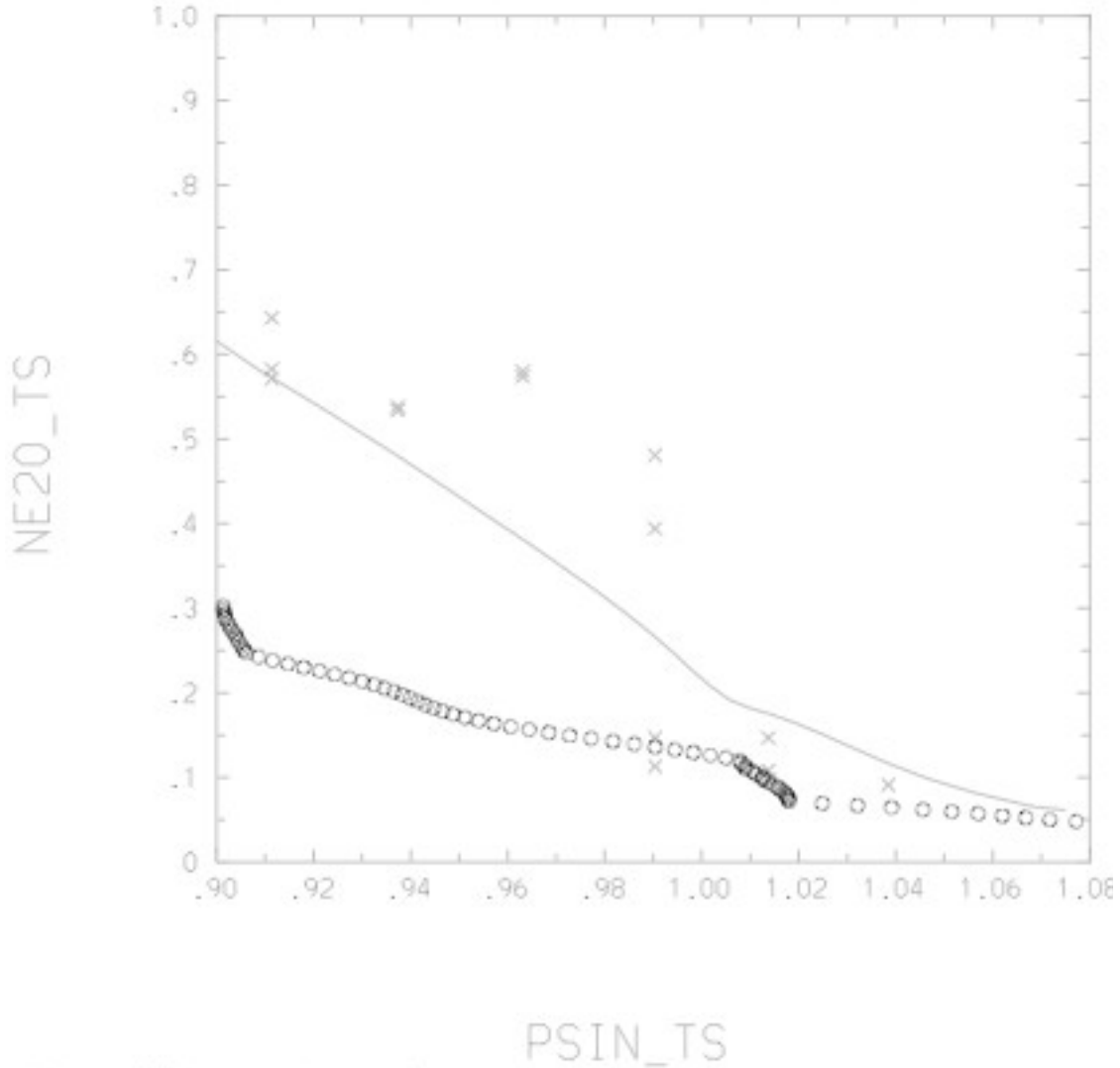


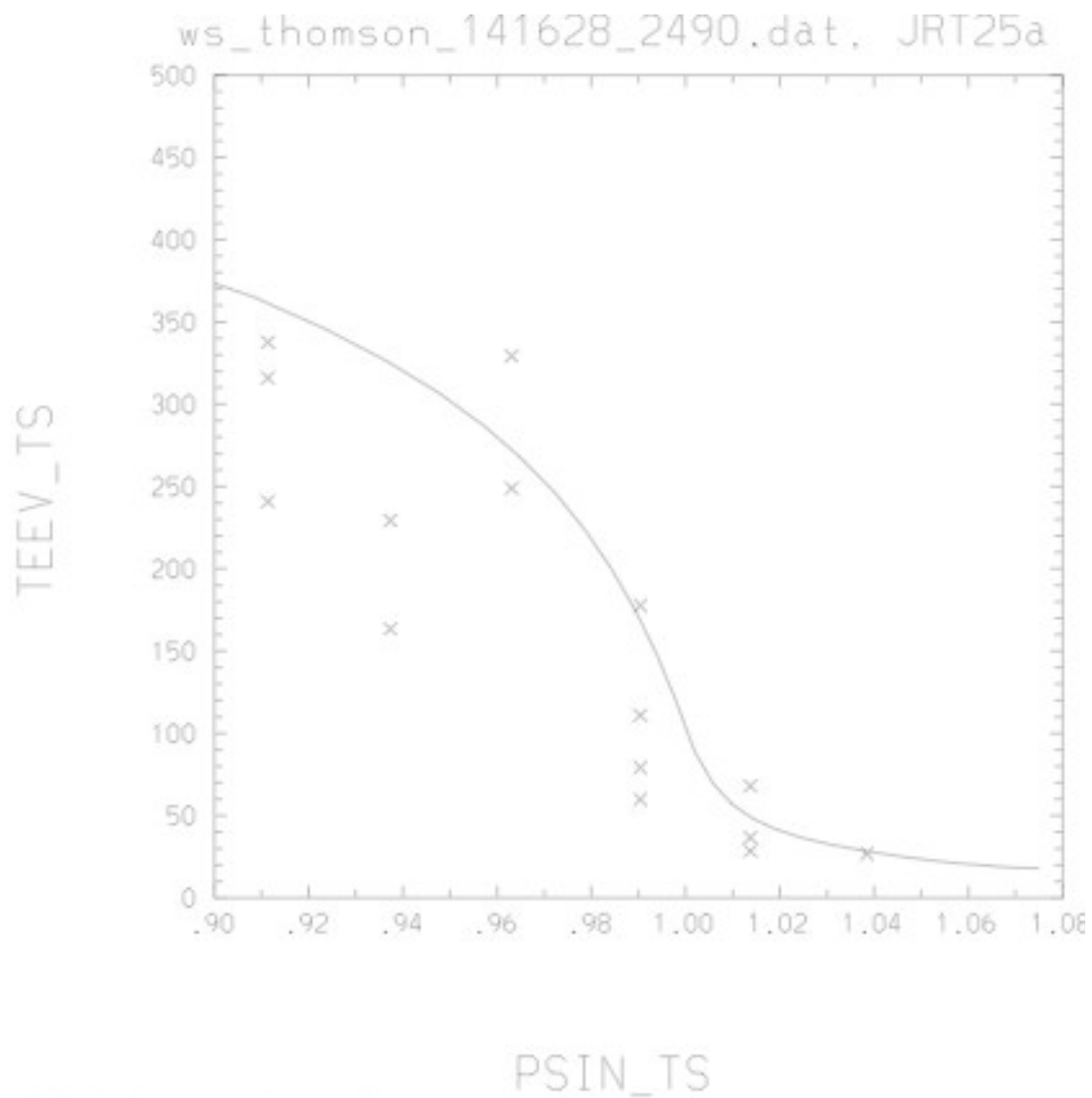
Fig. 2: Mesh for UEDGE simulations

ws_thomson_141628_2490.dat, JRT25a



```
plot ne20ts psints mark=cross  
plot tsne20 tspsin labels=blank  
plot densrefl psinrefl mark=circle
```

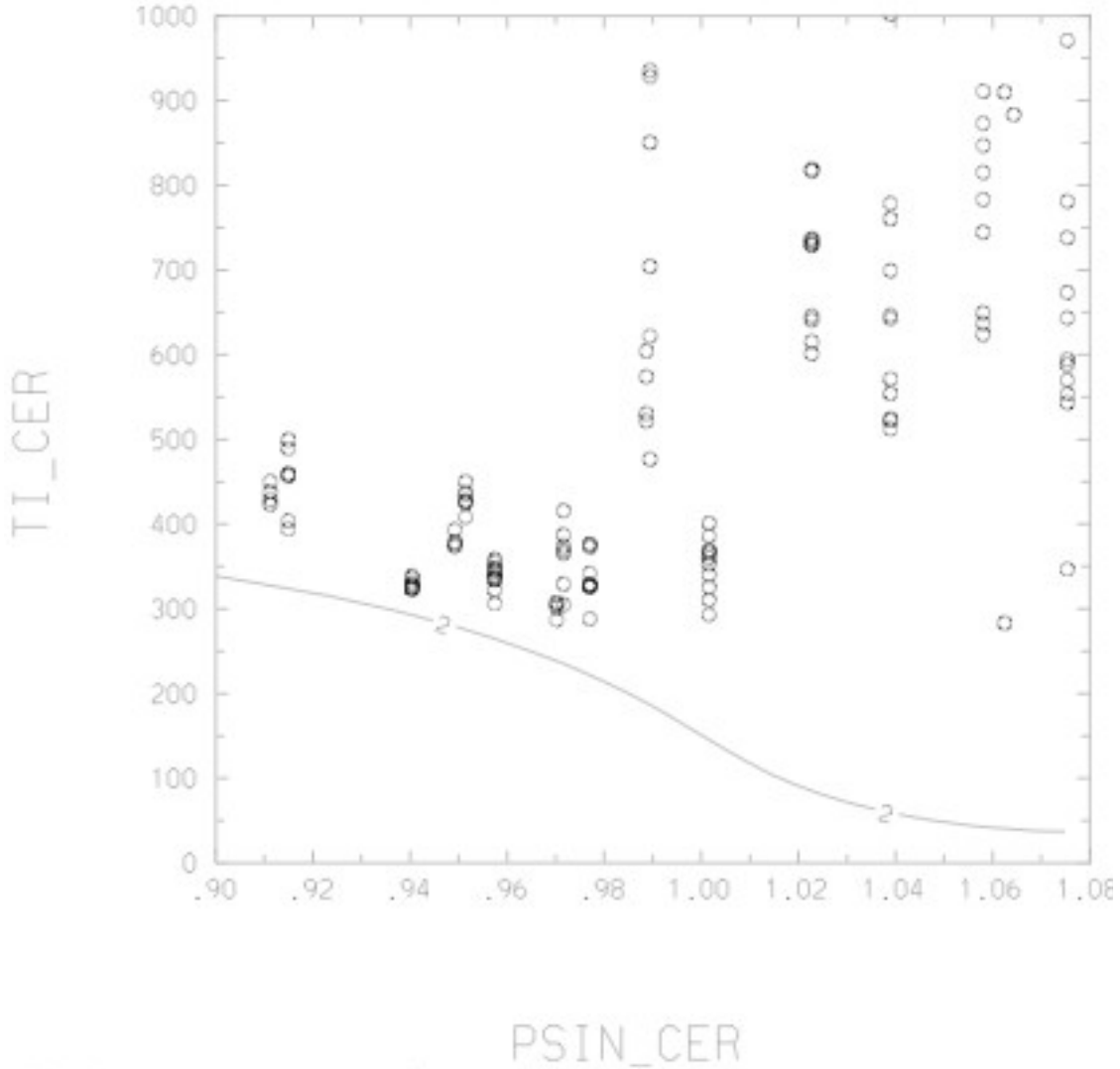
Fig. 3: upstream electron density profile



```
plot tets psints mark=cross
plot tsteev tspsin labels=blank
```

Fig. 4: upstream electron temperature profile

ws_cerauto_141628_2490.dat, JRT25a



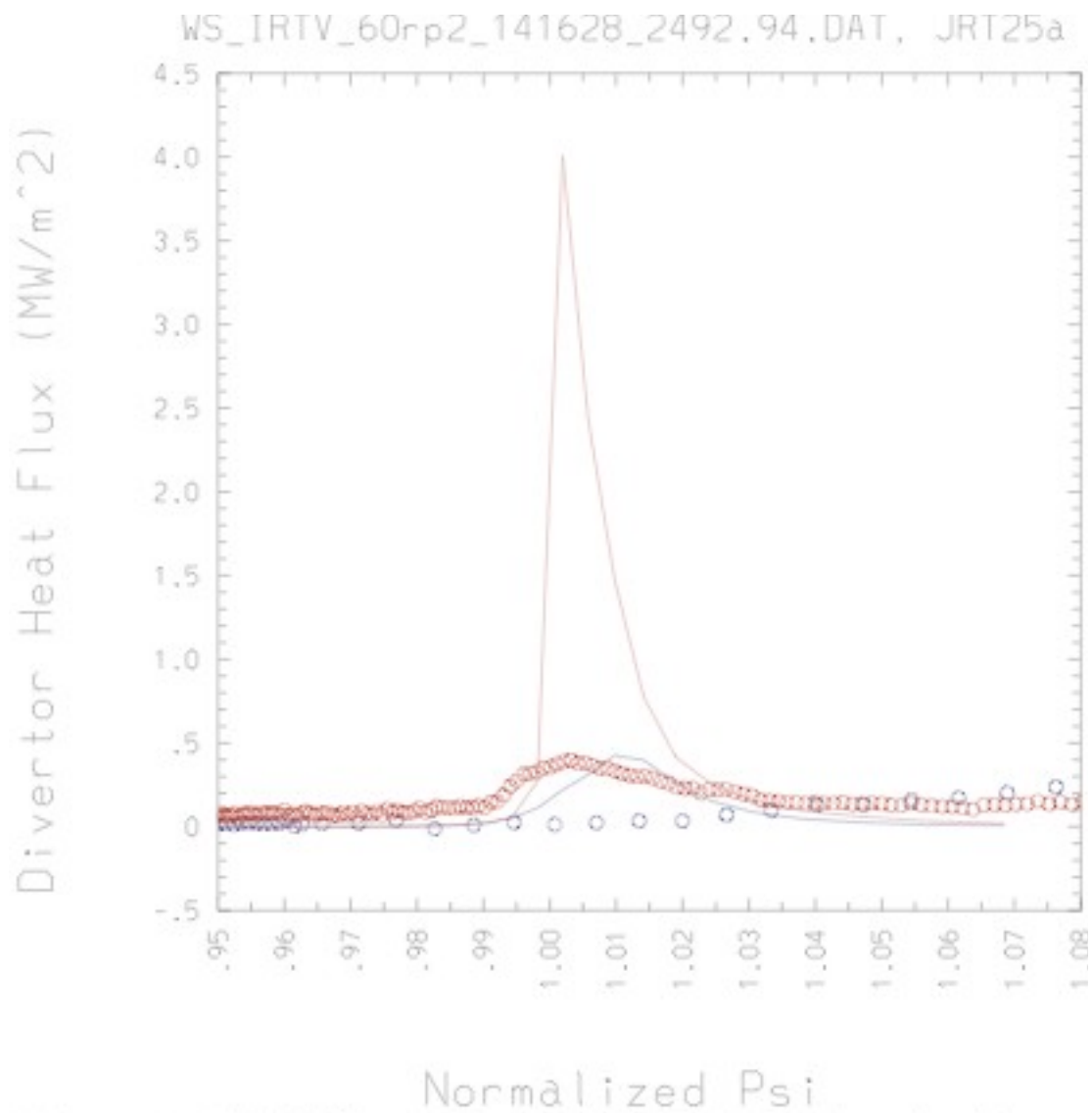


Fig. 6: divertor heat flux profile

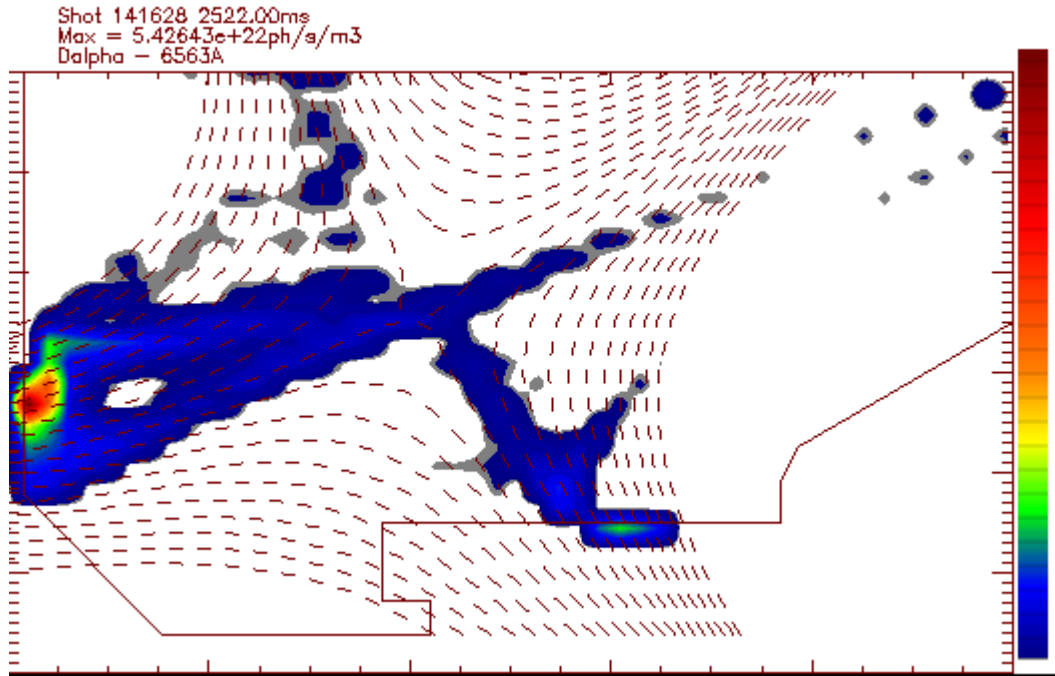


Fig. 7: Dalpha emissivity from visible TV

Dalpha 6563A, JRT25a

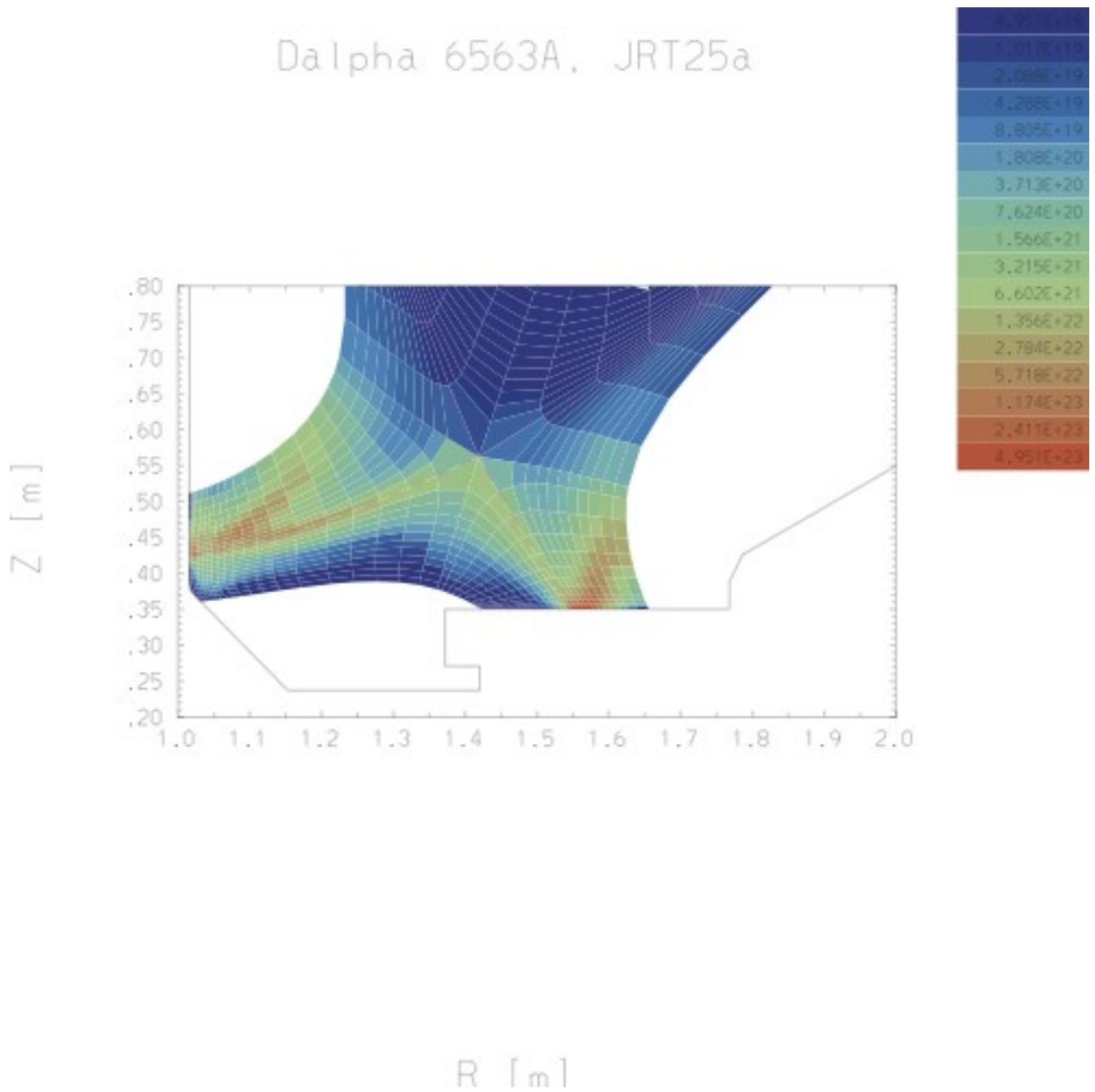


Fig. 8: Dalpha emissivity from UEDGE simulation JRT25a

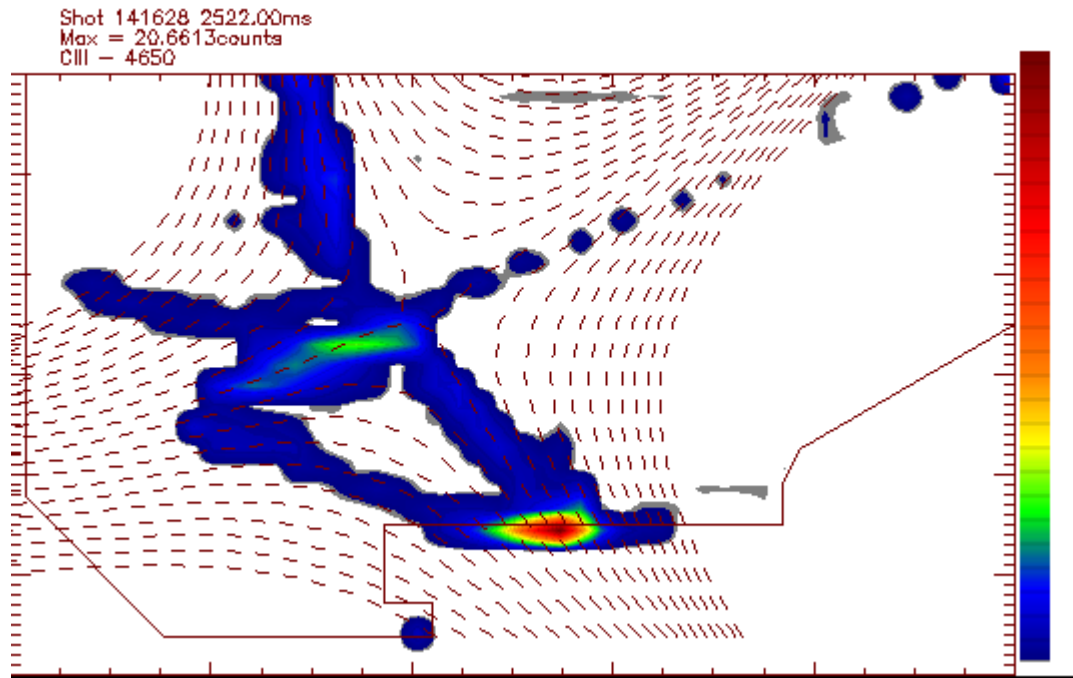


Fig. 9: CIII emissivity from visible TV

CIII 4650A, JRT25a

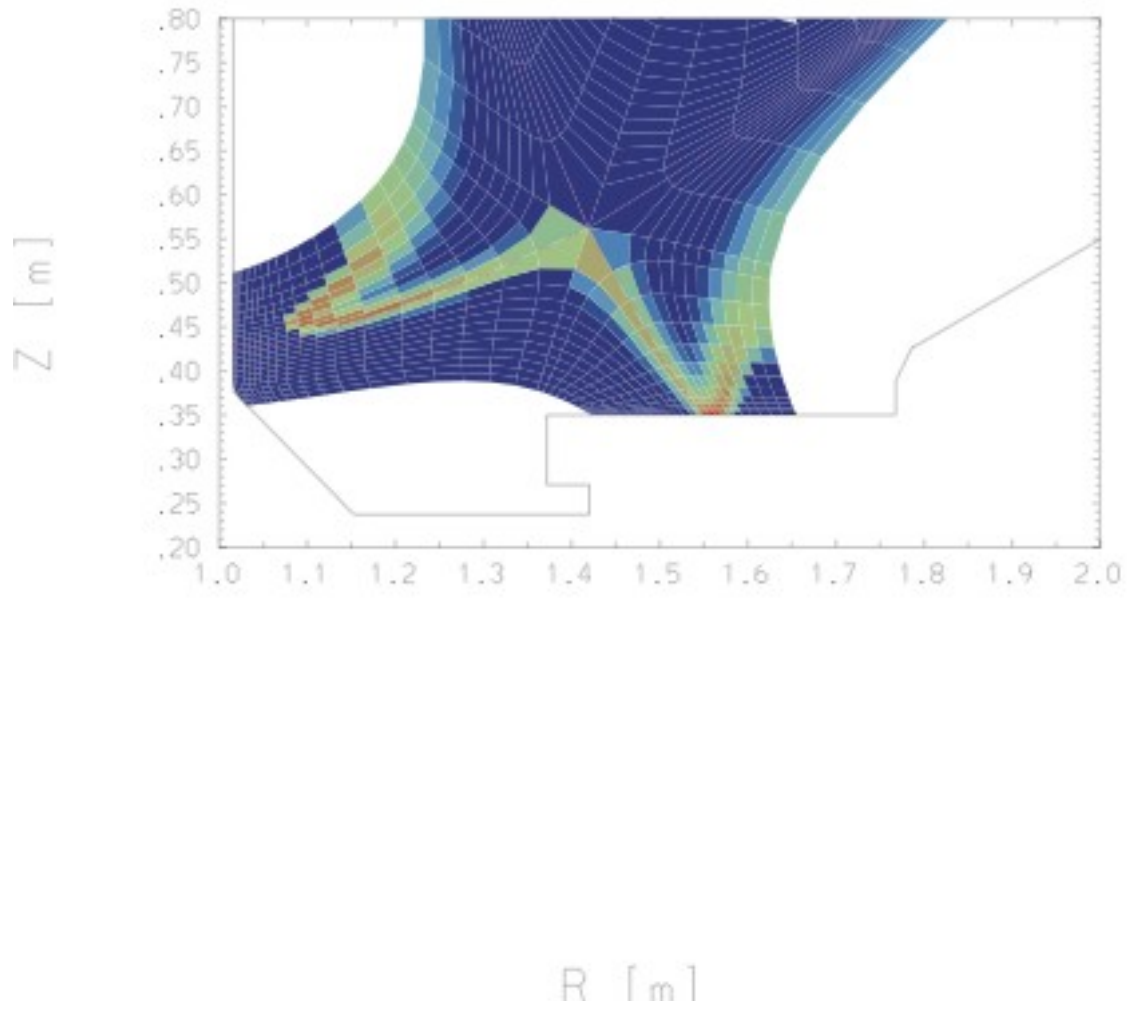
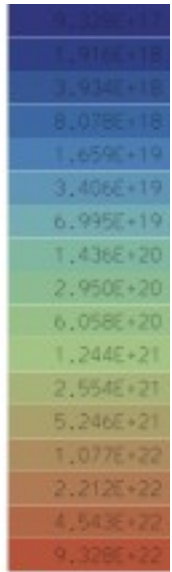


Fig. 10: CIII emissivity from UEDGE simulation JRT25a